Liver adapts mitochondrial function to insulin resistant and diabetic states in mice

Andras Franko[1,2,3#], Jürgen-Christoph von Kleist-Retzow[1,4,5#], Susanne Neschen[2,3], Moya Wu[2,3], Philipp Schommers[1], Marlen Böse[1], Alexander Kunze[6], Ursula Hartmann[6], Carmen Sanchez-Lasheras[7], Oliver Stoehr[8], Michael Huntgeburth[9], Susanne Brodesser[10,11], Martin Irmler[2], Johannes Beckers[2,3,12], Martin Hrabě de Angelis[2,3,12], Mats Paulsson[5,6,11], Markus Schubert[5,8,11]* and Rudolf J. Wiesner[1,5,11]*

[1] Center for Physiology and Pathophysiology, Institute for Vegetative Physiology, University of Köln, 50931 Köln, Germany

[2] Institute of Experimental Genetics, Helmholtz Zentrum München GmbH, 85764 Neuherberg, Germany

[3] German Center for Diabetes Research (DZD), 85764, Neuherberg, Germany

[4] Department of Pediatrics, University of Köln, 50924 Köln, Germany

[5] Center for Molecular Medicine Cologne, CMMC, University of Köln, 50931 Köln, Germany

[6] Department of Biochemistry, University of Köln, 50931 Köln, Germany

[7] Department of Mouse Genetics and Metabolism, Institute for Genetics, University of Köln, 50674 Köln, Germany

[8] Center for Endocrinology, Diabetes and Preventive Medicine, University of Köln, 50937 Köln, Germany

[9] Department of Internal Medicine III, University of Köln, 50937 Köln, Germany

[10] Institute for Medical Microbiology, Immunology and Hygiene, University of Köln, 50935 Köln, Germany

[11] Cologne Excellence Cluster on Cellular Stress Responses in Aging-associated Diseases (CECAD), 50674 Köln, Germany

[12] Technische Universität München, WZW - Center of Life and Food Science Weihenstephan, Chair of Experimental Genetics, 85350 Freising-Weihenstephan, Germany

# equal contribution

* these two authors are both corresponding authors rudolf.wiesner@uni-koeln.de or markus.schubert@uni-koeln.de

Contact Information:

Prof. Rudolf J. Wiesner, PhD, Center for Physiology and Pathophysiology, University of Köln, Robert-Koch-Str. 39, 50931 Köln, Germany, Tel: +49 221 478 3610, FAX: +49 221 478 6965; rudolf.wiesner@uni-koeln.de

Word count: 5309 words

4 Figures and 2 Tables

List of Abbreviations

HFD: high fat diet; STZ: streptozocin; IR: insulin receptor; IRS: insulin receptor substrate; RC: respiratory chain. TCC: tricarboxylic acid cycle

The authors have no conflict of interest to declare.

Financial Support

This work was initially funded by the intramural Köln Fortune Program on Diabesity (MS, RJW), the Forschergruppe "Basement membrane composition in the normal and diabetic retina" (DFG PA660/10-1: MP), the Center for Molecular Medicine Cologne (CMMC: JCvKR, MS, RJW), the Cologne Excellence Cluster on Cellular Stress Responses in Aging-associated Diseases (CECAD: UH, MP, MS, RJW) and by a grant from the German Federal Ministry of Education and Research (BMBF) to the German Center for Diabetes Research (DZD e.V.: MHDA, JB, SN, MW).

Abstract

Background&Aims

To determine if diabetic and insulin-resistant states cause mitochondrial dysfunction in liver or if there is long term adaptation of mitochondrial function to these states, mice were (i) fed with a high-fat diet to induce obesity and T2D (HFD), (ii) had a genetic defect in insulin signaling causing whole body insulin resistance, but not full blown T2D (IR/IRS-1+/- mice) or (iii) were analyzed after treatment with streptozocin (STZ) to induce a T1D-like state.

Methods

Hepatic lipid levels were measured by thin layer chromatography. Mitochondrial respiratory chain (RC) levels and function were determined by Western blot, spectrophotometric, oxygen consumption and proton motive force analysis. Gene expression was analyzed by real-time PCR and microarray.

Results

HFD caused insulin resistance and hepatic lipid accumulation, but RC was largely unchanged. Livers from insulin resistant IR/IRS-1+/- mice had normal lipid contents and a normal RC, but mitochondria were less well coupled. Livers from severely hyperglycemic and hypoinsulinemic STZ mice had massively depleted lipid levels, but RC abundance was unchanged. However, liver mitochondria isolated from these animals showed increased abundance and activity of the RC, which was better coupled.

Conclusions

Insulin resistance, induced either by obesity or genetic manipulation and steatosis do not cause mitochondrial dysfunction in mouse liver. Also, mitochondrial dysfunction is not a prerequisite for liver steatosis. However, severe insulin deficiency and high blood glucose levels lead to an enhanced performance and better coupling of the RC. This may represent an adaptation to fuel overload and the high energy-requirement of an unsuppressed gluconeogenesis.

Word count: 250 words

Key words

Type 2 diabetes mellitus, Mitochondrial biogenesis, Mitochondrial gene expression, Insulin receptor, Liver metabolism.

Introduction

The liver is intimately involved in the pathogenesis of diabetes, where hepatic insulin resistance is regarded as a key contributing element to high fasting blood glucose [1] and ketone body formation and thus to the development of diabetic complications. Insulin resistance has been attributed to the ectopic deposition of lipids in liver and muscle [2] [3], and mitochondrial dysfunction has been proposed to be the underlying cause for this lipid overload [4]. Indeed, delayed recovery from fructose-induced ATP depletion pointed to mitochondrial dysfunction in the liver of patients with steatohepatitis [5]. Moreover, low activities of respiratory chain (RC) complexes were measured in liver biopsies of patients with nonalcoholic fatty liver [6], a condition observed in about 70% of patients with obesity or type 2 diabetes [7]. Thus, impaired energy metabolism may lead to hepatic insulin resistance and could even precede the development of hepatic steatosis in type 2 diabetes. More recently, in lean patients with type 2 diabetes, magnetic resonance spectroscopy showed lower hepatocellular ATP concentrations, which were related to low hepatic insulin sensitivity, but not to hepatocellular lipid volumes [3].

In the light of the importance of disturbed energy homeostasis and, in particular, mitochondrial dysfunction in the pathogenesis of type 2 diabetes and insulin resistance, we investigated liver mitochondrial function in three mouse models in which glucose and lipid metabolism is affected by different mechanisms. The mice were studied at about 6 months of age or treatment, i.e. after long term insulin resistance, in order to mimic the situation encountered in the majority of patients. Even at this advanced stage, we did not observe RC dysfunction in any of our models. Therefore, no obvious relation exists between insulin signaling and mitochondrial function in the liver, in contrast to muscle, where we recently showed a severe mitochondrial impairment in muscle specific insulin receptor knockout mice (MIRKO) as well as in the same cohort of STZ mice used here [8]. However, after STZ treatment, we found an elevated capacity for substrate oxidation and a decreased mitochondrial proton leak in isolated organelles, while total

hepatocellular mitochondrial content remained unchanged. We propose that this may represent an important adaptation to the fuel overload and the high energy-requirement of an unsuppressed gluconeogenesis.

Materials and methods

Animal studies

All animal studies were approved by local government authorities (Bezirksregierung Köln/LANUV). Exposure to HFD and STZ treatment, glucose and insulin tolerance tests as well as analyis of serum insulin levels, serum triglyceride and cholesterol levels were performed as described recently [8]. IR/IRS-1+/- mice [9] were generated by crossing mice heterozygous for insulin receptor null [10] and IRS-1 null alleles [11] respectively, into the same C57BL/6N background. All mice were sacrifed at the age of 6 months. HFD mice were fed with HFD for 5 months. STZ was injected i.p. at a dose of 60 mg/kg for five consecutive days and mice were analyzed 2 months later. In order to show hepatic insulin resistance, insulin (1.5 U/kg; Humulin R, Lilly, Indianapolis, USA) was injected i.p. in two new cohorts of HFD and IR/IRS-1+/- mice, the animals were sacrificed by cervical dislocation 10 min later, the liver was rapidly removed and frozen in liquid nitrogen before measuring the phosphorylation state of Akt. In order to show hepatic insulin resistance in STZ mice euglycemic-hyperinsulinemic clamps were performed (see Supplementary Information).

Mitochondrial RC function

Liver mitochondria were prepared by differential centrifugation [12]. The final pellet was resuspended in polarography buffer (sucrose 250mM, Tris 20mM, EDTA 2mM, KCl 40mM, BSA 0.3%). Oxygen consumption studies were performed as described before [13]. Mitochondrial proton motive force was determined by measuring the membrane potential $\Delta\Psi$ in freshly isolated mitochondria using a methyltriphenylphosphonium TPMP ion-sensitive electrode, while analyzing

in parallel the respiration rate with a Clark type electrode (Rank Bros., Cambridge, United Kingdom), in a proton leak titration assay as described in [14].

Measurement of mitochondrial enzyme activities

The carnitine palmitoyl transferase 1 (CPT-1) activity was determined as described in [12]. Since liver contains other malonyl-CoA insensitive enzymes beside CPT-2, only CPT-1 activity values are given. Spectrophotometric measurements of the TCA cycle enzymes citrate synthase (CS), isocitrate dehydrogenase (IDH), aconitase and fumarase were performed in liver homogenates using a Varian Cary 50 spectrophotometer (Varian Instruments, Mulgrave, Australia) by standard methods [15] [16].

Western blots

Western blots of whole liver extracts (10 µg of protein) or liver mitochondria (2 µg of protein) were prepared. Antibodies were purchased from Cell Signaling (P-Ser^{473}AKT, total AKT), Life Technologies (RC antibodies), Biomol (MnSOD), Calbiochem (UCP-2), Sigma (β-actin), BD Biosciences (HSP-60), Santa Cruz (ANT) and used as described [8].

Lipid extraction and Thin Layer Chromatography analysis

Lipids were extracted from frozen liver samples and analyzed as described [17].

Real time PCR

See Supplementary Information.

Microarray

Amplification and array processing (human Affymetrix Gene ST 1.0) were done as previously described [18]. Expression console (Affymetrix, High Wycombe, United Kingdom) was used to obtain normalized RNA gene-level data. Statistical analysis was performed in CARMAweb [19]. Genewise testing for differential expression was done employing the t-test option and Benjamini-Hochberg multiple testing correction (FDR<10%). Pathway enrichment analysis was done with Ingenuity Pathway software.

Other Statistics

All data were compared using the two-tailed Student´s t-test assuming unequal distribution. O'Brien´s OLS (ordinary least squares) test [20] was used to compare Western blot signals of complex I, III and IV subunits.

Results

Mouse models

We have previously shown that in muscle, complete failure of insulin-transmitted signaling in STZ treated as well as in muscle-insulin-receptor knockout mice impairs RC function, while obesity-induced insulin resistance in leptin deficient ob/ob or in HFD mice has no effect [8]. Here, we have used the same cohorts of HFD and STZ-mice as well as genetically induced, insulin resistant mice (whole body IR/IRS-1+/- mice; animal data see Table 1) to determine whether the RC is affected in the liver. Suggesting impaired insulin signalling in liver a decrease in the phospho-Akt^{473}/Akt ratio was observed in HFD-fed animals and in IR/IRS-1+/- mice compared to their respective controls [9] (Suppl. Fig. 1A-B). Euglycemic hyperinsulinemic clamp studies were performed in fully conscious, freely moving and widely undisturbed mice. STZ treated mice expressed a markedly decreased whole body insulin sensitivity compared to untreated mice (GIR, Suppl. Fig 1E). This was accompanied by the reduced ability of insulin to suppress endogenous glucose production rates (EndoRa) from basal values in STZ treated compared to untreated individuals (Suppl. Fig 1F). However, negative EndoRa values, frequently observed when hepatic glucose production is measured with the tracer-dilution technique during the euglycemic hyperinsulinemic glucose clamp, were calculated in control mice under insulin stimulation. To directly compare groups, a single insulin dose was chosen that was effective in lowering blood glucose concentrations in the highly insulin-resistant STZ treated mice but caused considerably higher GIRs in insulin-sensitive untreated individuals. Thus, negative EndoRa values might be related to marked differences in insulin sensitivity and glucose turnover in both

groups, an underestimation of glucose disposal by using the conventional “cold” (tracer-free) glucose infusion method (as the EndoRa is calculated from the difference between tracer-derived glucose disposal and GIR), arterio-venous differences in tracer concentrations and other factors. However, glucose clamp studies clearly indicate impaired hepatic insulin action in STZ treated mice compared to untreated littermates.

Hepatic lipid levels do not influence the abundance and expression of the mitochondrial OXPHOS system

HFD led to a marked accumulation of diacylglycerols and a 5-fold increase of triglycerides, but not free fatty acids (Fig. 1A). This did not change levels of mitochondrial OXPHOS proteins (Fig. 2A and Suppl. Fig. 2A). On the contrary, treatment with STZ led to severe depletion of hepatic diacylglycerols, triglycerides and also free fatty acids (Fig. 1B), which however did not change steady state levels of the mitochondrial OXPHOS system in liver homogenates as well (Fig. 2B and Suppl. Fig. 2B). No differences in lipid (Suppl. Fig. 3) or OXPHOS protein levels (Fig. 2C and Suppl. Fig. 2C) were observed in liver homogenates of IR/IRS-1+/- mice.

Expression of genes for representative subunits for each of the five OXPHOS complexes, when analyzed by quantitative RT-PCR, was unchanged in HFD mice (Suppl. Fig. 4A). In STZ mice, we observed a small but significant decrease in mRNA levels of CI and CIV subunits (Suppl. Fig. 4C), however expression of other complexes remained unaltered. Also, the expression of heme oxygenase (Hox-1) was not altered in either model (Suppl. Figs. 4B and 4D). This enzyme was previously shown to be induced in liver-specific IRS-1/IRS-2 double knockout mice, as well as in db/db and ob/ob mice and was postulated to disrupt the RC via heme depletion [21]. The mRNA levels of PGC-1α, CPT-1A, CPT-2 as well as UCP-2 were found to be similar in HFD and STZ mice compared to their respective controls (Suppl. Fig. 4B and 4D).

Adaptation of intrinsic mitochondrial activity to insulin resistant and diabetic states

Isolated liver mitochondria from HFD mice showed similar oxygen consumption as controls when using the substrates malate and pyruvate that feed electrons into complex I. However, a

significantly increased capacity to oxidize glycerol-3-phosphate, feeding electrons into the quinone pool before complex III, was found (Fig. 3A). Mitochondria of HFD mice showed a decreased state IVo respiration (Suppl. Table 1). The levels of OXPHOS complexes in HFD mice were similar to controls when normalized to the high abundance mitochondrial matrix protein Hsp-60 (Fig. 3B-C). Also, the level of the main superoxide scavenger MnSOD was unchanged. In contrast, liver mitochondria of STZ mice showed a small, but significant, increase of oxygen consumption when electrons were channeled into complex I (Fig. 3D), which was mirrored by a significantly higher steady state level of complex I (Fig. 3E-F). Since complexes I, III and IV are strongly interdependent and assembled into supercomplexes or respirasomes [22], it is reasonable to assume that their steady state levels change in parallel. Using O´Brien´s OLS test, we assessed coordinated changes of these complexes, and found a significant, about 3-fold increase of these complexes ($p = 0.0136$, denoted by # in Fig. 3F). Also, complex II levels were significantly elevated while levels of MnSOD were unchanged (Fig. 3E-F). Thus, when normalized to the high abundance matrix protein Hsp-60, we found higher steady state levels of all OXPHOS complexes in isolated organelles.

A defect in insulin signaling in IR/IRS-1+/- mice caused a significant decrease in oxygen consumption with succinate as the complex II substrate, but not with other substrates (Fig. 3G). This was reflected in a marked albeit not significant decrease of complex II levels (Fig. 3H-I), while other complexes were unchanged. Also the level of the main superoxide scavenger MnSOD was similar.

The activity of carnitine-palmitoyltransferase 1 (CPT-1), the enzyme responsible for transferring cytosolic acyl-CoAs to carnitine, thus shuttling fatty acids into the mitochondrial matrix, was unchanged in all models (Table 2). In order to assess the capacity of the tricarboxylic acid cycle, the activities of citrate synthase (CS), isocitrate dehydogenase (IDH) and fumarase were measured. HFD led to an increased activity of all three enzymes (Table 2).

Changes in proton motive force and levels of uncoupling protein-2 (UCP-2) and adenine nucleotide translocator (ANT)

Liver mitochondria from IR/IRS-1+/- mice showed a higher proton leak compared to their wt littermates, best evidenced when comparing the respiratory rates at the highest common membrane potential ($\Delta\psi$) during proton leak titration assays [23] (Fig. 4C). On the contrary, although liver mitochondria from HFD mice showed slightly decreased proton leak, the titration curves almost overlapped (Fig. 4A). This indicates only subtle changes in proton conductance and likely a reduction in substrate oxidation as previously suggested [23]. Liver mitochondria of STZ-mice showed decreased proton leak as well and were able to generate a higher membrane potential ($\Delta\psi$) compared to their respective controls (Fig. 4B).

Although it is debated whether UCP-2, the ubiquitously expressed UCP-1 homologue, is indeed involved in proton leak [24] [25], we decided to analyze its levels in isolated mitochondria. In addition, we studied steady state levels of the adenine nucleotide transporter (ANT), which is also implicated in basal proton conductance over the inner mitochondrial membrane. Both proteins were marginally increased in mitochondria from STZ mice, they were unchanged in HFD animals and UCP-2 displayed a decreased level in IR/IRS-1+/- mice (Suppl. Fig. 5 and Suppl. Table 2). In order to verify the specificity of the UCP-2 antibody used, isolated mitochondria from UCP-2 knock-out mice were also loaded (Suppl. Fig. 5D).

Global gene expression in livers of STZ treated mice

In order to find putative causes for and pathways leading to the differences in mitochondrial performance observed in isolated mitochondria from livers of type 1 diabetic STZ mice, we analyzed global gene expression using mRNA arrays. Microarray data was submitted to GEO (GSE39752) and a link for review has been created:

http://www.ncbi.nlm.nih.gov/geo/query/acc.cgi?token=tjepjskgicyeaxk&acc=GSE39752.

No differences in the expression of nuclear genes encoding mitochondrial RC proteins were noted (data not shown), supporting our RT-PCR measurements (Suppl. Fig. 4). Unchanged levels of mRNAs for OXPHOS genes reflect unchanged levels of OXPHOS proteins in liver tissue, as expected, since tissue abundance of the RC is importantly dictated by corresponding mRNA levels [26] [27] [28].

In general, changes of other proteins and enzymes involved in the pathways of interest to us were small and confirm that these livers are in a state of enhanced gluconeogenesis, kataplerosis as well as fatty acid oxidation (Suppl. Table 3). Expression of the transcriptional coactivator PGC-1α, which has been shown to stimulate the gluconeogenesis pathway upon starvation [29], was increased 2-fold, in accordance with a 1.5-fold increase of the PEPCK mRNA, a key gluconeogenetic enzyme. The antagonistically acting PPARγ, which also suppresses lipogenesis [30], was downregulated. Increased expression of the transaminases GOT and GPT and the mitochondrial glutamate/aspartate exchanger (Slc25a12 or aralar) was observed, which probably serves to increase conversion of amino acids into TCC intermediates. Also, expression of the mitochondrial oxoglutarate and malate dehydrogenases was enhanced, all pointing to an increased flux of carbon from amino acids to phosphoenolpyruvate to support gluconeogenesis. The NADP dependent cytosolic malic enzyme was decreased by 70%, while the mitochondrial isoform was upregulated, again probably in order to support anaplerotic reactions. Increased hepatic oxidation of fatty acids was reflected by coordinated, enhanced expression of the plasma membrane fatty acid transporter CD36, some fatty acid binding proteins (FABP), although appointed to other organs according to the database, and the mitochondrial fatty acid transporter Slc27a1. Expression of NADP-dependent isocitrate-dehydrogenase (NADP-IDH) was increased, probably in order to provide NADPH for the mitochondrial glutathione system. Expression of glucokinase was markedly downregulated, probably in order to avoid massive channeling of excess glucose into fuel metabolism, and the monocarboxylic acid transporters Slc16a5 and

Slc16a19 were markedly increased, probably in order to import pyruvate and lactate for gluconeogenesis.

Discussion

Several clinical studies have implicated that hepatocellular steatosis and mitochondrial dysfunction may be intimately related [3] [5] [6] summarized previously by [2]. Thus, it was proposed that liver mitochondrial dysfunction may be the underlying cause for hepatic insulin resistance, as it was postulated for muscle [4]. Indeed, mitochondrial dysfunction induced in mouse liver by expressing a hypomorphic variant of the transcriptional co-activator PGC-1ß resulted in hepatic insulin resistance [31]. Also, mice with only one functional PGC1-α allele in the liver had increased steatosis with decreased expression of mitochondrial ß-oxidation enzymes, high serum triglycerides and hepatic insulin resistance [32]. However, in liver PGC1-α mainly regulates the gluconeogenetic program upon starvation, in contrast to muscle, heart and brown adipose tissue, where this coactivator is importantly involved in physiological upregulation of the mitochondrial biogenesis program, while PGC-1ß shows a wide tissue distribution and is thought to be a main regulator of this program in many cell types [33]. On the contrary, inducing mild mitochondrial dysfunction in liver by ablation of the RC complex I associated subunit AIF increased glucose tolerance, even upon HFD [34]. In addition, a microarray study showed that in livers of patients with type 2 diabetes, genes involved in the RC pathway were upregulated, together with genes involved in gluconeogenesis, ß-oxidation and transcription factors associated with energy homeostasis [35]. A longitudinal study in mice indicated that the liver may initially adapt to HFD, since genes involved in fatty acid oxidation were upregulated 4 weeks after the start of HFD, but downregulated at 10 weeks, while lipogenic genes showed opposite trends [36]. Levels of mtDNA and expression of mitochondrial genes were decreased after 8 weeks of HFD in mice [37]. In conclusion, it seems that the liver is flexible and adapts its energy metabolism and

mitochondrial performance to pre-diabetic and diabetic states, and that the time between the onset of the insult and analysis as well as the severity of the insult is extremely important for the outcome.

In order to mimic the situation in typical type 2 diabetic patients as close as possible, we decided to study mice that had been exposed to a HFD for 5 months. We conclude from our results that the severe hepatic steatosis induced by this treatment does not result in dysfunction of the RC system, but rather results in an adaptive response with even increased activities of TCC cycle enzymes (Table 2) and an augmented capacity to oxidize glycerol-3-phosphate derived from triglycerides (Fig. 3A). The activity of CPT-1 was unchanged (Table 2), demonstrating that the enzyme is present in sufficient amounts in liver, in contrast to skeletal muscle where HFD stimulated expression of this mitochondrial fatty acid shuttle enzyme [8] [38]. Since the oxidation of lipids, probably the preferred fuel under HFD, generates more ATP per electron channeled into the RC than carbohydrates, we saw a tendency for less oxidation of succinate as a substrate (Fig. 3A), while proton leak and proton conductance over the IMM were basically unchanged (Fig. 4A). *Vice versa*, our results strongly support the concept that mitochondrial dysfunction is not a necessary prerequisite for steatosis, since massive lipid accumulation was observed in the presence of normal mitochondrial function. Therefore, we postulate that low levels of ATP and decreased activities of RC complexes observed in livers from type 2 diabetic patients [3] must be an inherited trait or due to other factors, but are not caused primarily by mitochondrial dysfunction.

Also, a whole body genetic defect in insulin signaling (IR/IRS-1+/-) did not cause a decrease in levels of RC subunits (Fig. 2C). Interestingly, liver mitochondria of IR/IRS-1+/- mice were less well coupled, and indeed total body heat production of these animals was significantly higher than controls (Kunze et al., in preparation). Thus, it seems that the IR-IRS signaling cascade affects mitochondrial efficiency, but not mitochondrial mass. However, this mechanism is not recapitulated in full blown type 2 diabetes after HFD. Uncoupling of liver mitochondria may

significantly contribute to whole body energy production, especially in mice, where the liver contributes to about 7% of the body mass in contrast to humans (2%). However, even with this completely different relation, liver and muscle each contribute one quarter of the resting energy expenditure in humans and in rodents [39]. Thus uncoupling of liver mitochondria by mild disturbance of the IR-IRS signaling cascade may be an important means of increasing energy expenditure also in man, and may underlie the beneficial effect of such manipulations on healthy life span [40].

Although no changes in the steady state levels of mitochondrial proteins were detected in liver homogenates of severely diabetic STZ mice (Fig. 2B), isolated organelles showed increased activity and levels of RC complexes and even better coupling (Figs 3D-F and 4B). Interestingly, better coupling was also observed by others in mitochondria isolated from heart and skeletal muscle of severely diabetic rats 2 months after STZ treatment [41]. This was considered an adaptation to preceding oxidative stress, which is postulated to be an important cause of diabetic complications [42] [43]. Mitochondrial superoxide production was indeed unchanged in these rats. The same explanation may apply to the liver mitochondria of STZ mice used in our study, where we found no significant changes in the levels of the main superoxide scavenger MnSOD, which is regularly increased upon oxidative stress, and the ROS sensitive enzyme aconitase. However, since we also found increased RC complexes, but not TCC enzyme activities in isolated organelles, we propose that this is not the only cause for better performance of mitochondria under such conditions. Rather we postulate that under conditions of extremely low insulin, the capacity of the liver TCC is decreased due to cataplerosis of TCC intermediates, which are “used up” for gluconeogenesis. An energetic deficit inside the mitochondria results, which is compensated by increasing RC and coupling by reducing proton leak in the organelle, without changing the total tissue content. Mechanistically, the reduced proton leak in STZ liver mitochondria may be due to the low levels of free fatty acids, which are naturally occurring uncouplers.

Acknowledgements

We acknowledge Dr. Martin Hellmich (Institute of Medical Statistics, Informatics and Epidemiology, University of Köln) for advice with statistical analyses, especially with O'Brien´s OLS test. We also thank Prof. Jens Brüning (Department of Mouse Genetics and Metabolism, University of Köln) for providing IRS-1+/- and IR+/- mice and Maria Bust, Anett Seelig and Jürgen Schultheiß for excellent technical assistance.

Reference list

[1] Campbell PJ, Mandarino LJ, Gerich JE. Quantification of the relative impairment in actions of insulin on hepatic glucose production and peripheral glucose uptake in non-insulin-dependent diabetes mellitus. Metabolism 1988;37:15-21.
[2] Szendroedi J, Roden M. Ectopic lipids and organ function. CurrOpinLipidol 2009;20:50-56.
[3] Szendroedi J, Chmelik M, Schmid AI, Nowotny P, Brehm A, Krssak M, et al. Abnormal hepatic energy homeostasis in type 2 diabetes. Hepatology 2009;50:1079-1086.
[4] Lowell BB, Shulman GI. Mitochondrial dysfunction and type 2 diabetes. Science 2005;307:384-387.
[5] Cortez-Pinto H, Chatham J, Chacko VP, Arnold C, Rashid A, Diehl AM. Alterations in liver ATP homeostasis in human nonalcoholic steatohepatitis: a pilot study. JAMA : the journal of the American Medical Association 1999;282:1659-1664.
[6] Perez-Carreras M, Del Hoyo P, Martin MA, Rubio JC, Martin A, Castellano G, et al. Defective hepatic mitochondrial respiratory chain in patients with nonalcoholic steatohepatitis. Hepatology 2003;38:999-1007.
[7] Farrell GC, Larter CZ. Nonalcoholic fatty liver disease: from steatosis to cirrhosis. Hepatology 2006;43:S99-S112.
[8] Franko A, von Kleist-Retzow JC, Bose M, Sanchez-Lasheras C, Brodesser S, Krut O, et al. Complete failure of insulin-transmitted signaling, but not obesity-induced insulin resistance, impairs respiratory chain function in muscle. Journal of molecular medicine (Berlin, Germany) 2012;90:1145-1160.
[9] Bruning JC, Winnay J, Bonner-Weir S, Taylor SI, Accili D, Kahn CR. Development of a novel polygenic model of NIDDM in mice heterozygous for IR and IRS-1 null alleles. Cell 1997;88:561-572.
[10] Accili D, Drago J, Lee EJ, Johnson MD, Cool MH, Salvatore P, et al. Early neonatal death in mice homozygous for a null allele of the insulin receptor gene. Nature genetics 1996;12:106-109.
[11] Araki E, Lipes MA, Patti ME, Bruning JC, Haag B, III, Johnson RS, et al. Alternative pathway of insulin signalling in mice with targeted disruption of the IRS-1 gene. Nature 1994;372:186-190.
[12] Kerner J, Parland WK, Minkler PE, Hoppel CL. Rat liver mitochondrial carnitine palmitoyltransferase-I, hepatic carnitine, and malonyl-CoA: effect of starvation. ArchPhysiol Biochem 2008;114:161-170.
[13] Rustin P, Chretien D, Bourgeron T, Gerard B, Rotig A, Saudubray JM, et al. Biochemical and molecular investigations in respiratory chain deficiencies. Clinica chimica acta; international journal of clinical chemistry 1994;228:35-51.

[14] Brand MD. Measurement of mitochondrial protonmotive force. Bioenergetics 1995:39-62.
[15] Geromel V, Rotig A, Munnich A, Rustin P. Coenzyme Q10 depletion is comparatively less detrimental to human cultured skin fibroblasts than respiratory chain complex deficiencies. Free RadicRes 2002;36:375-379.
[16] Bourgeron T, Chretien D, Poggi-Bach J, Doonan S, Rabier D, Letouze P, et al. Mutation of the fumarase gene in two siblings with progressive encephalopathy and fumarase deficiency. JClinInvest 1994;93:2514-2518.
[17] Belgardt BF, Mauer J, Wunderlich FT, Ernst MB, Pal M, Spohn G, et al. Hypothalamic and pituitary c-Jun N-terminal kinase 1 signaling coordinately regulates glucose metabolism. Proc Natl Acad Sci U S A 2010;107:6028-6033.
[18] Baumhoer D, Zillmer S, Unger K, Rosemann M, Atkinson MJ, Irmler M, et al. MicroRNA profiling with correlation to gene expression revealed the oncogenic miR-17-92 cluster to be up-regulated in osteosarcoma. Cancer genetics 2012;205:212-219.
[19] Rainer J, Sanchez-Cabo F, Stocker G, Sturn A, Trajanoski Z. CARMAweb: comprehensive R- and bioconductor-based web service for microarray data analysis. Nucleic acids research 2006;34:W498-503.
[20] O'Brien PC. Procedures for comparing samples with multiple endpoints. Biometrics 1984;40:1079-1087.
[21] Cheng Z, Guo S, Copps K, Dong X, Kollipara R, Rodgers JT, et al. Foxo1 integrates insulin signaling with mitochondrial function in the liver. NatMed 2009;15:1307-1311.
[22] Schagger H, Pfeiffer K. Supercomplexes in the respiratory chains of yeast and mammalian mitochondria. The EMBO journal 2000;19:1777-1783.
[23] Divakaruni AS, Brand MD. The regulation and physiology of mitochondrial proton leak. Physiology 2011;26:192-205.
[24] Mailloux RJ, Harper ME. Uncoupling proteins and the control of mitochondrial reactive oxygen species production. Free Radic Biol Med 2011;51:1106-1115.
[25] Shabalina IG, Nedergaard J. Mitochondrial ('mild') uncoupling and ROS production: physiologically relevant or not? Biochemical Society transactions 2011;39:1305-1309.
[26] Gagnon J, Kurowski TT, Wiesner RJ, Zak R. Correlations between a nuclear and a mitochondrial mRNA of cytochrome c oxidase subunits, enzymatic activity and total mRNA content, in rat tissues. Molecular and cellular biochemistry 1991;107:21-29.
[27] Wiesner RJ. Regulation of mitochondrial gene expression: transcription versus replication. Trends in genetics : TIG 1992;8:264-265.
[28] Wiesner RJ, Hornung TV, Garman JD, Clayton DA, O'Gorman E, Wallimann T. Stimulation of mitochondrial gene expression and proliferation of mitochondria following impairment of cellular energy transfer by inhibition of the phosphocreatine circuit in rat hearts. JBioenergBiomembr 1999;31:559-567.
[29] Herzig S, Long F, Jhala US, Hedrick S, Quinn R, Bauer A, et al. CREB regulates hepatic gluconeogenesis through the coactivator PGC-1. Nature 2001;413:179-183.
[30] Herzig S, Hedrick S, Morantte I, Koo SH, Galimi F, Montminy M. CREB controls hepatic lipid metabolism through nuclear hormone receptor PPAR-gamma. Nature 2003;426:190-193.
[31] Vianna CR, Huntgeburth M, Coppari R, Choi CS, Lin J, Krauss S, et al. Hypomorphic mutation of PGC-1beta causes mitochondrial dysfunction and liver insulin resistance. Cell Metab 2006;4:453-464.
[32] Estall JL, Kahn M, Cooper MP, Fisher FM, Wu MK, Laznik D, et al. Sensitivity of lipid metabolism and insulin signaling to genetic alterations in hepatic peroxisome proliferator-activated receptor-gamma coactivator-1alpha expression. Diabetes 2009;58:1499-1508.
[33] Gupta RK, Rosen ED, Spiegelman BM. Identifying novel transcriptional components controlling energy metabolism. Cell Metab 2011;14:739-745.
[34] Pospisilik JA, Knauf C, Joza N, Benit P, Orthofer M, Cani PD, et al. Targeted deletion of AIF decreases mitochondrial oxidative phosphorylation and protects from obesity and diabetes. Cell 2007;131:476-491.

[35] Takamura T, Misu H, Matsuzawa-Nagata N, Sakurai M, Ota T, Shimizu A, et al. Obesity upregulates genes involved in oxidative phosphorylation in livers of diabetic patients. Obesity(SilverSpring) 2008;16:2601-2609.
[36] Chan MY, Zhao Y, Heng CK. Sequential responses to high-fat and high-calorie feeding in an obese mouse model. Obesity (Silver Spring) 2008;16:972-978.
[37] Liu HY, Hong T, Wen GB, Han J, Zuo D, Liu Z, et al. Increased basal level of Akt-dependent insulin signaling may be responsible for the development of insulin resistance. Am J Physiol Endocrinol Metab 2009;297:E898-906.
[38] Garcia-Roves P, Huss JM, Han DH, Hancock CR, Iglesias-Gutierrez E, Chen M, et al. Raising plasma fatty acid concentration induces increased biogenesis of mitochondria in skeletal muscle. ProcNatlAcadSciUSA 2007.
[39] Rolfe DF, Brown GC. Cellular energy utilization and molecular origin of standard metabolic rate in mammals. Physiological reviews 1997;77:731-758.
[40] Fontana L, Partridge L, Longo VD. Extending healthy life span--from yeast to humans. Science 2010;328:321-326.
[41] Herlein JA, Fink BD, O'Malley Y, Sivitz WI. Superoxide and respiratory coupling in mitochondria of insulin-deficient diabetic rats. Endocrinology 2009;150:46-55.
[42] Nishikawa T, Edelstein D, Du XL, Yamagishi S, Matsumura T, Kaneda Y, et al. Normalizing mitochondrial superoxide production blocks three pathways of hyperglycaemic damage. Nature 2000;404:787-790.
[43] Brownlee M. The pathobiology of diabetic complications: a unifying mechanism. Diabetes 2005;54:1615-1625.

Tables

Table 1. Body weight and serum glucose, insulin and lipid levels
Serum insulin, triglyceride and cholesterol levels were determined in 16 hours fasted mice and their respective controls. Data are expressed as mean±SD, n=3-6,
*p<0.05, **p<0.01, ***p<0.001; [a]fed insulin levels, [b]minimal value obtained, no mean calculated as several values were higher than 600 mg/dl, the upper detection limit of the instrument used. Part of these data have been published previously [8].

		Body weight [g]	Fasted glucose [mg/dl]	Random fed glucose [mg/dl]	Fasted insulin [ng/ml]	Triglycerides [mg/dl]
HFD	Control	29.1±1.3	95.8±9.4	149.0±13.1	0.2±0.1	47.0±17.4
	Treated	50.1±2.8***	168.0±21.3***	143.7±8.8	7.2±1.4***	84.0±8.2**
IR/IRS-1+/-	Control	33.3±1.8	116.9±4.0	143.4±4.4	0.7 [a]±0.1	81.6±10.7
	IR/IRS-1+/-	28.4±1.9***	99.4±3.4**	146.1±9.5	2.2[a]±0.3***	70.8±11.9*
STZ	Control	31.7±2.3	112.0±33.8	167.8±15.4	0.7±0.3	108.5±17.1
	Treated	22.0±2.3***	257.0±32.0**	>475[b]	0.1±0.02*	87.0±40.2

Table 2. Activities of the TCC cycle enzymes and CPT-1
TCC enzyme activities were measured in liver homogenates, CPT-1 in liver mitochondria. Data are expressed as mean±SD, n=5, *p<0.05, **p<0.01, ***p<0.001. [a]p=0.0575, nd=not determined

		CS [nmol/min/mg]	IDH [nmol/min/mg]	Fumarase [nmol/min/mg]	Aconitase [nmol/min/mg]	CPT-1 [dpm]
HFD	Control	146.1±14.3	237.7±11.8	359.8±47.6	59.0±10.3	4074.4±499.2
	Treated	220.9±20.0***	275.3±20.5*	442.7±67.0[a]	69.0±10.7	4770.3±597.9
IR/IRS-1+/-	Control	170.4±9.7	235.6±16.2	370.5±28.4	nd	1554.2±327.4
	IR/IRS-1+/-	164.5±16.4	209.6±30.2	423.4±78.4	nd	1440.0±466.0
STZ	Control	119.7±19.5	121.9±13.9	217.1±28.6	57.9±2.8	3195.8±289.9
	Treated	108.9±29.5	127.3±22.9	407.6±69.6**	68.6±9.2	3343.3±448.3

Figure legends

Fig. 1 Lipid analysis

Thin layer chromatography of liver homogenates of **(A)** HFD and **(B)** STZ mice; chromatograms (upper panel) and their quantitative analysis (lower panel). Results are expressed as mean±SD, n=4, *p<0.05, **p<0.01. (DAG=Diacylglycerol; Cho=cholesterol; CL=cardiolipin; FFA=free fatty acids; PC=Phosphatidylcholine; PE=Phosphytidylethanolamine; PI/PS=Phosphatidyl-inositol/Phosphatidylserine; TG=triglycerides)

Fig. 2 Steady state levels of RC components

Steady-state levels of representative subunits of the five RC complexes (I–V) in liver tissue from **(A)** HFD, **(B)** STZ treated and **(C)** IR/IRS-1+/- mice. For quantification after normalization to beta-actin see Suppl. Fig. 2.

Fig. 3 Oxygen consumption and steady state levels of mitochondrial proteins in liver mitochondria of HFD, STZ and IR/IRS-1+/- mice

(A,D,G) Oxygen consumption (substrates: MPox=pyruvate/malate, MGox=malate/glutamate; Sox=succinate, GPox=glycerol-3-phosphate) and **(B,E,H)** steady-state levels of representative complex subunits (CoI–V) and MnSOD in liver mitochondria after normalization to HSP-60 **(C,F,I).** Results are expressed as mean±SD, n=3-8, *p<0.05, **p<0.01, ***p<0.001. Levels of complex I, III and IV, assembled as supercomplexes, were compared to controls using O´Brien´s OLS test, $^{\#}$p<0.05. The values for state IVo respiration are shown in Suppl. Table 1.

Fig. 4 Proton motive force

Proton leak kinetics in isolated liver mitochondria of **(A)** HFD, **(B)** STZ treated and **(C)** IR/IRS-1+/- mice and respective controls as determined by simultaneous titration of succinate respiration and

mitochondrial membrane potential ($\Delta\Psi$) using increasing amounts of the respiratory inhibitor malonate. To perceive more easily the respective changes in proton conductance, we labeled the respiration at the highest common membrane potential in all three models and their respective controls. Results are expressed as mean±SEM, n=4-7 animals, each kinetics was measured twice, *p<0.05 when comparing $\Delta\Psi$ at same level of graded inhibition of succinate respiration; #p<0.05, ##p<0.01 when comparing respiration at same level of graded inhibition of succinate respiration.

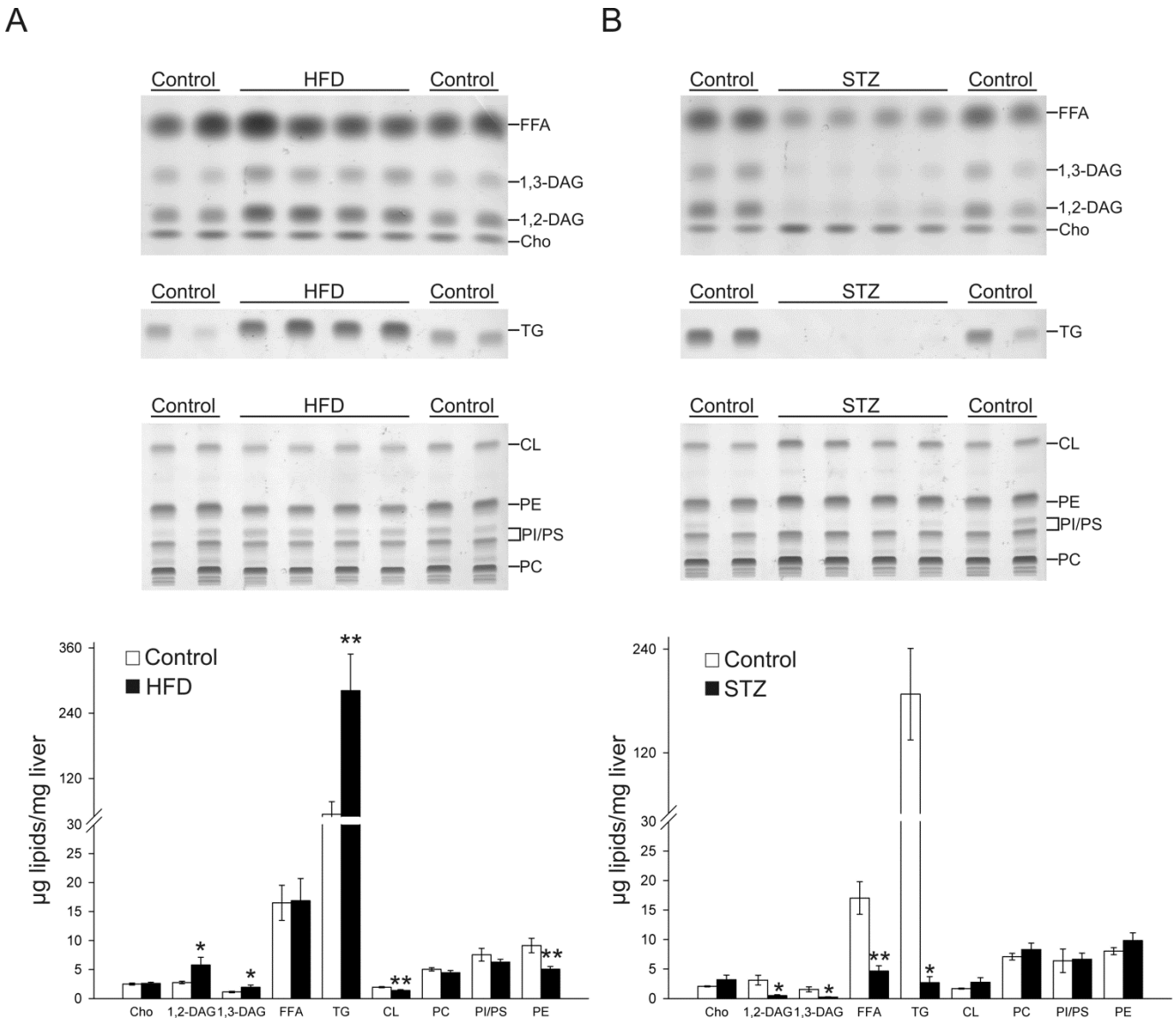
A
B
Control
HFD
STZ
FFA
1,3-DAG
1,2-DAG
Cho
TG
CL
PE
PI/PS
PC
μg lipids/mg liver
Cho
1,2-DAG
1,3-DAG
FFA
TG
CL
PC
PI/PS
PE

Figure 1

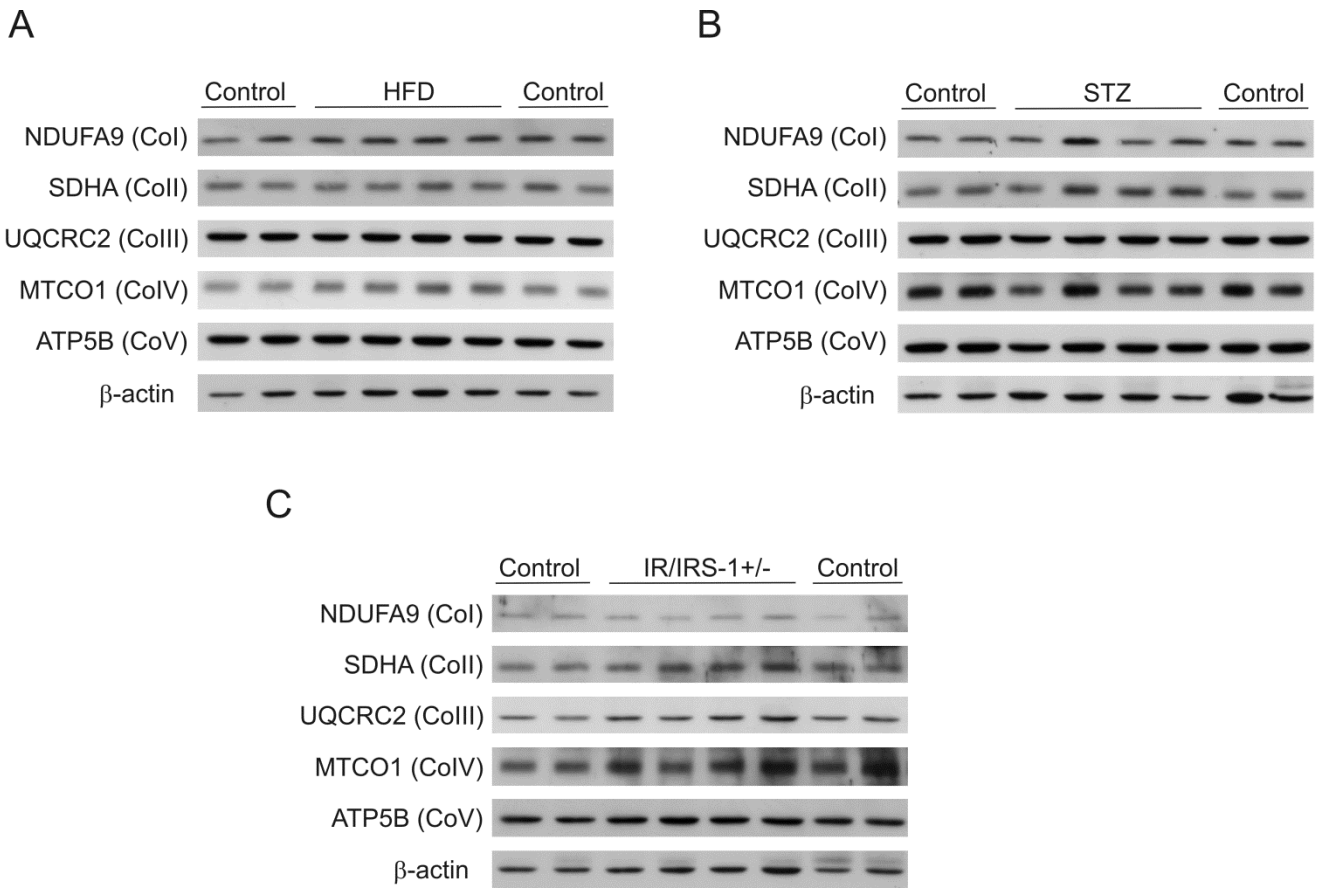
A
Control
HFD
Control
NDUFA9 (CoI)
SDHA (CoII)
UQCRC2 (CoIII)
MTCO1 (CoIV)
ATP5B (CoV)
β-actin
B
Control
STZ
Control
NDUFA9 (CoI)
SDHA (CoII)
UQCRC2 (CoIII)
MTCO1 (CoIV)
ATP5B (CoV)
β-actin
C
Control
IR/IRS-1+/-
Control
NDUFA9 (CoI)
SDHA (CoII)
UQCRC2 (CoIII)
MTCO1 (CoIV)
ATP5B (CoV)
β-actin

Figure 2

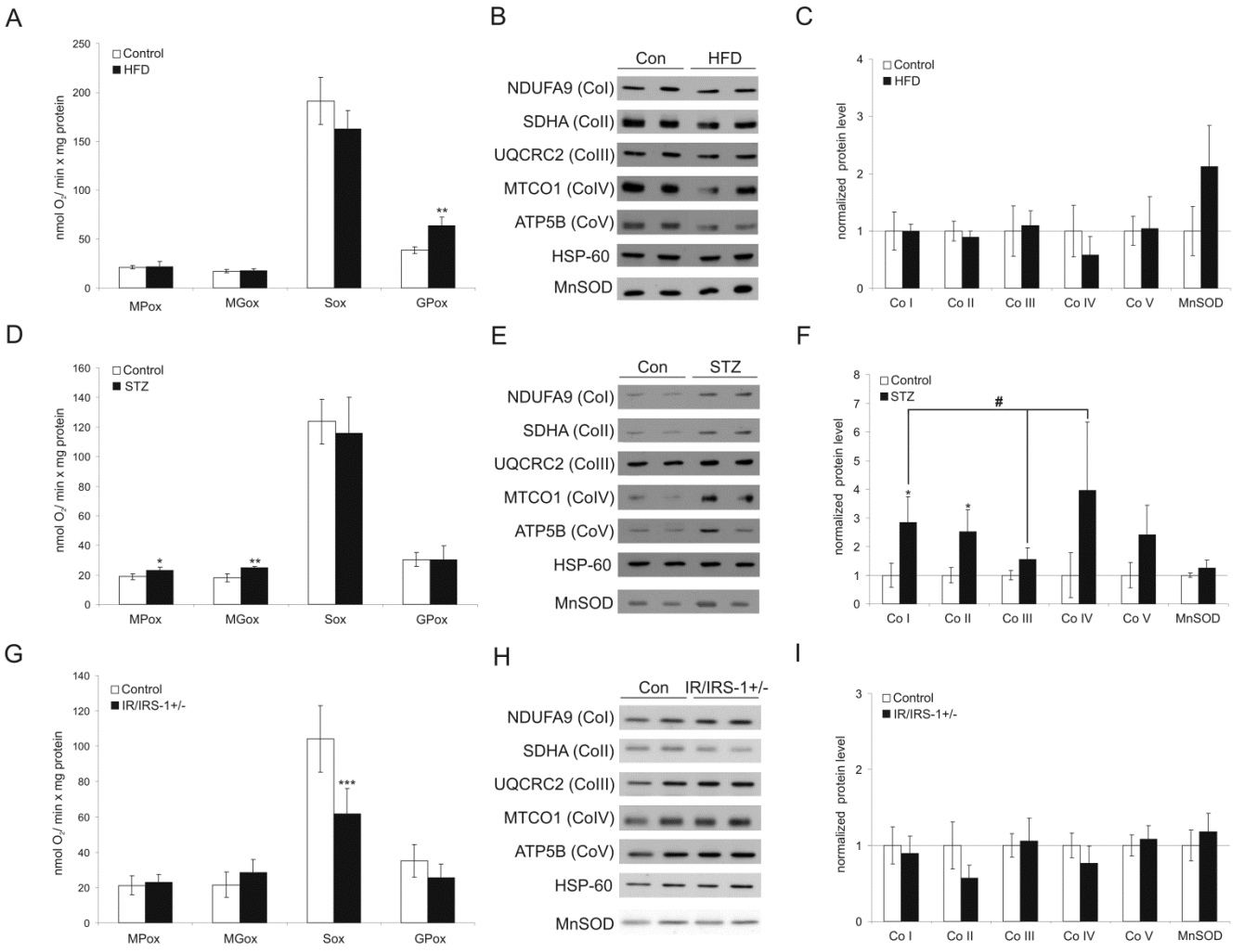
A
Control
HFD
nmol O2 / min x mg protein
MPox
MGox
Sox
GPox
B
Con
HFD
NDUFA9 (CoI)
SDHA (CoII)
UQCRC2 (CoIII)
MTCO1 (CoIV)
ATP5B (CoV)
HSP-60
MnSOD
C
Control
HFD
normalized protein level
Co I
Co II
Co III
Co IV
Co V
MnSOD
D
Control
STZ
E
Con
STZ
F
Control
STZ
G
Control
IR/IRS-1+/-
H
Con
IR/IRS-1+/-
I
Control
IR/IRS-1+/-

Figure 3

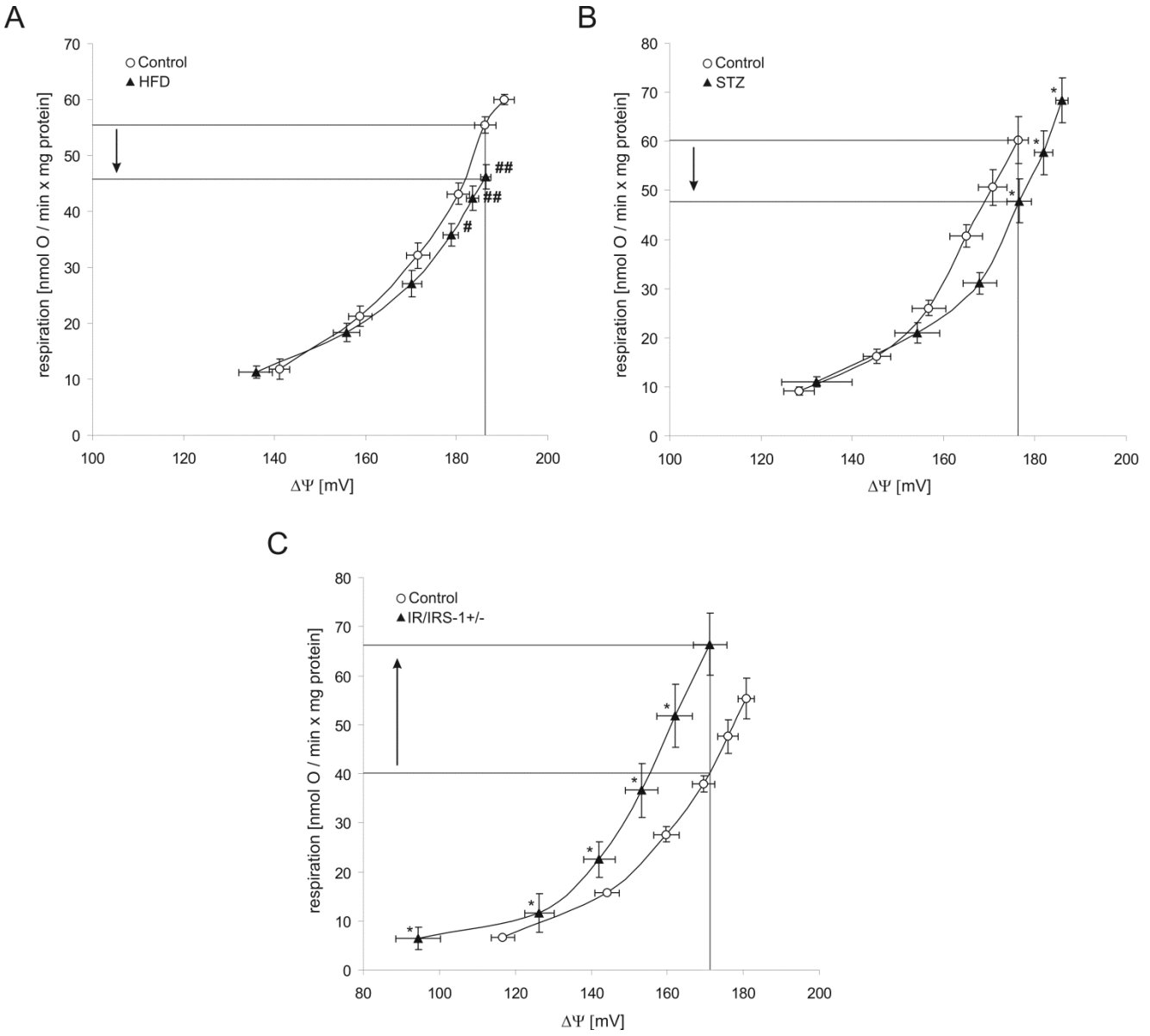
A
Control
HFD
respiration [nmol O / min x mg protein]
ΔΨ [mV]
B
Control
STZ
respiration [nmol O / min x mg protein]
ΔΨ [mV]
C
Control
IR/IRS-1+/-
respiration [nmol O / min x mg protein]
ΔΨ [mV]

Figure 4

Supplementary Figure 1 Liver of HFD, STZ and IR/IRS-1+/- mice show hepatic insulin resistance

Densitometric quantification of steady-state levels of phospho-Ser^{473} AKT normalized to total AKT level determined by Western blotting of liver homogenates from **(A)** HFD and **(B)** IR/IRS-1+/- mice. Results are expressed as mean±SD, n=3-5. Euglycemic-hyperinsulinemic clamp studies were conducted in mice 6 weeks after STZ injection **(C-F)**. **(C)** Random-fed blood glucose concentrations 2 to 4 weeks after STZ injection and prior to glucose clamp experiments. **(D)** Blood glucose concentrations during euglycemic-hyperinsulinemic clamps in body weight-matched groups of mice. **(E)** Glucose infusion rate (GIR) calculated for 30 minute time intervals. **(F)** Basal and insulin stimulated endogenous glucose production (EndoRa)**.** Results are expressed as mean±SD, n=5-8, **p<0.01, ***p<0.001.

Supplementary Figure 2 Steady state levels of RC components

Densitometric quantification of steady-state levels of proteins normalized to ß-actin representing the five RC complexes (I–V) determined by Western blotting of liver homogenates from **(A)** HFD, **(B)** STZ treated and **(C)** IR/IRS-1+/- mice. Results are expressed normalized to the respective ratio in controls (set to 1.0) as mean±SD, n=4. Ndufa9-complex I, Sdha-complex II, Uqcrc2-complex III, Mtco1-complex IV, Atp5b-complex V.

Supplementary Figure 3 Lipid analysis of IR/IRS-1+/- liver by thin layer chromatography (TLC)

Thin layer chromatography of liver homogenates of IR/IRS-1+/- mice and their respective controls. (1,2-DAG = 1,2-Diacylglycerol; 1,3-DAG = 1,3-Diacylglycerol; Cho = cholesterol; CL = cardiolipin; FFA = free fatty acids; PC = Phosphatidylcholine; PE = Phosphytidylethanolamine; PI/PS = Phosphatidylinositol/Phosphatidylserine; TG = triglycerides,). Chromatograms (upper panel) and their quantitative analysis

(lower panel; expressed as µg lipids/mg liver). Results are expressed as mean±SD, n=4.

Supplementary Figure 4 Expression of representative nuclear encoded mitochondrial genes, PGC-1α, UCP-2, CPT´s and heme oxygenase

Quantitative RT-PCR analysis of liver from **(A-B)** HFD, **(C-D)** STZ mice showing mRNA levels of representative subunits from RC complexes Co I–Co V, the heme oxygenase (Hmox), the transcriptional coactivator PGC-1α, uncoupling protein 2 (UCP-2) and key enzymes of the mitochondrial fatty acid oxidation, CPT1A and CPT2. Results were normalised to the housekeeping gene (GUSB) and to respective controls and expressed as mean±SD, n=3-4, *p<0.05, **p<0.01.

Supplementary Figure 5 Steady state levels of UCP2 and ANT

Steady-state levels of uncoupling protein 2 (UCP2) and adenine nucleotide transporter (ANT) determined by Western blotting of isolated liver mitochondria from **(A)** HFD, **(B)** STZ treated and **(C)** IR/IRS-1+/- mice. For quantification after normalization to HSP-60 see Suppl. Table 1. **(D)** Isolated spleen mitochondria from UCP-2 and UCP-3 knock-out mice, respectively, were used to verify the specificity of UCP-2 antibody.

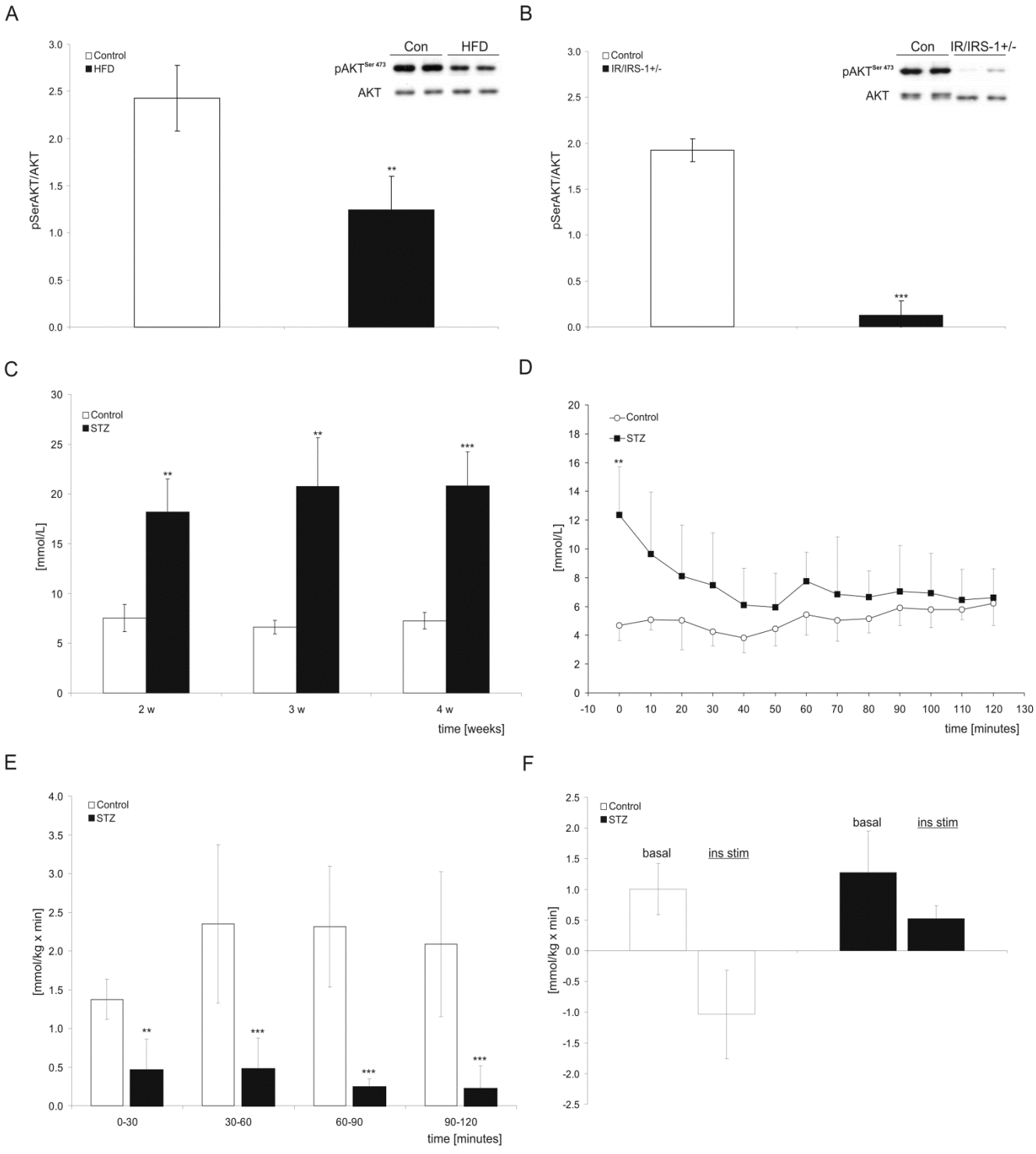
A
Control
HFD
Con
HFD
pAKT Ser 473
AKT
pSerAKT/AKT
**
B
Control
IR/IRS-1+/-
Con
IR/IRS-1+/-
pAKT Ser 473
AKT
pSerAKT/AKT
***
C
Control
STZ
[mmol/L]
**
**
***
2 w
3 w
4 w
time [weeks]
D
Control
STZ
[mmol/L]
**
time [minutes]
E
Control
STZ
[mmol/kg x min]
**
***
***
***
0-30
30-60
60-90
90-120
time [minutes]
F
Control
STZ
basal
ins stim
basal
ins stim
[mmol/kg x min]

Suppl. Fig. 1

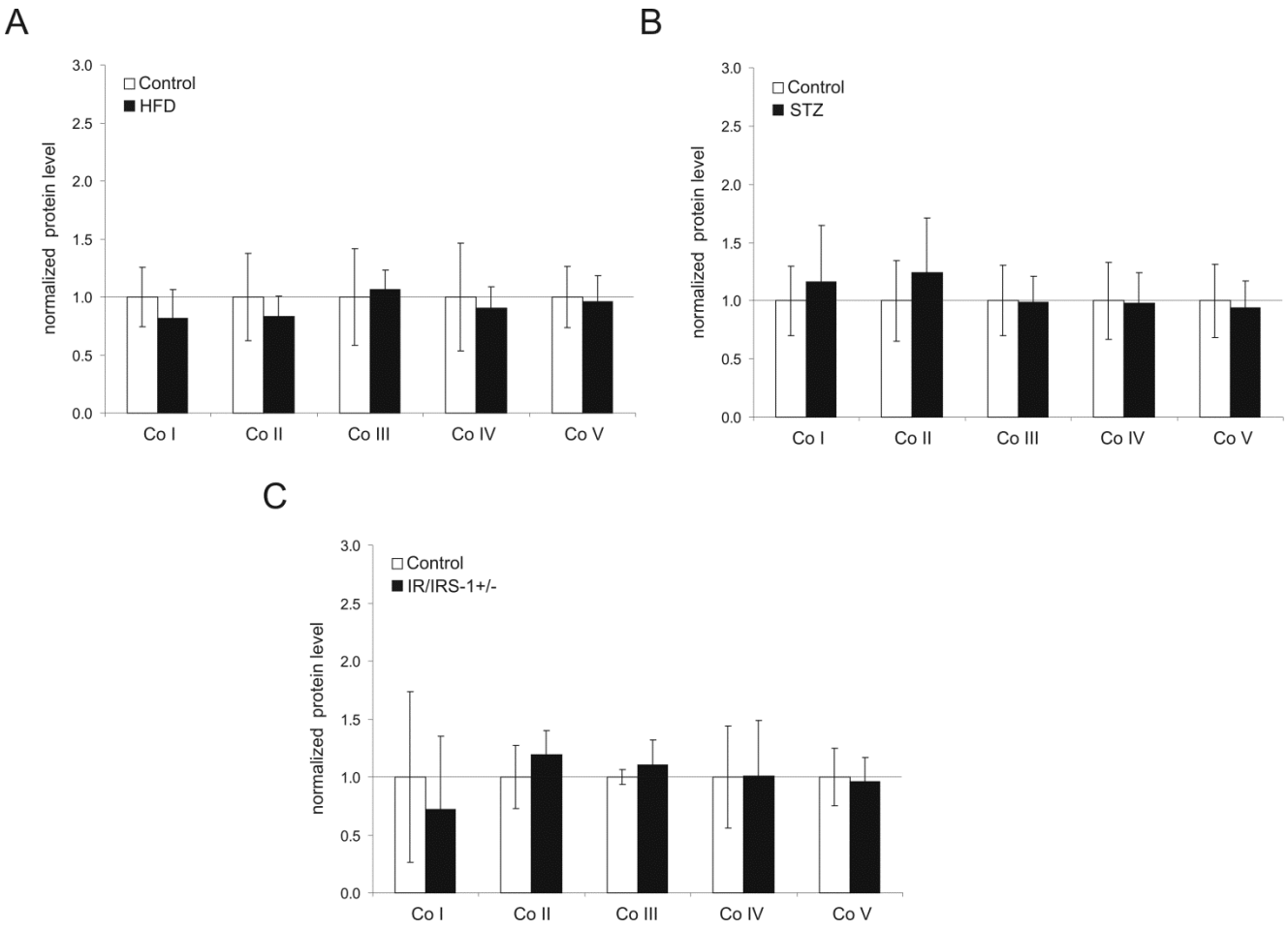
A
Control
HFD
normalized protein level
3.0
2.5
2.0
1.5
1.0
0.5
0.0
Co I
Co II
Co III
Co IV
Co V
B
Control
STZ
normalized protein level
3.0
2.5
2.0
1.5
1.0
0.5
0.0
Co I
Co II
Co III
Co IV
Co V
C
Control
IR/IRS-1+/-
normalized protein level
3.0
2.5
2.0
1.5
1.0
0.5
0.0
Co I
Co II
Co III
Co IV
Co V

Suppl. Fig. 2

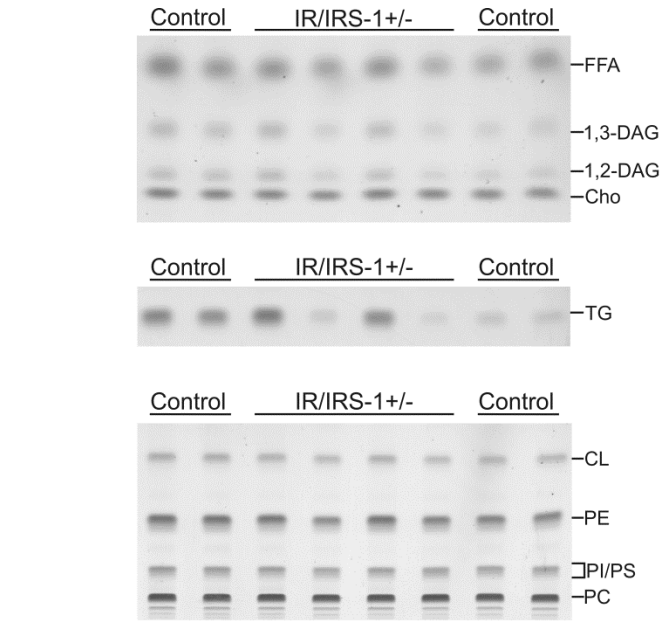
Control
IR/IRS-1+/-
Control
FFA
1,3-DAG
1,2-DAG
Cho
Control
IR/IRS-1+/-
Control
TG
Control
IR/IRS-1+/-
Control
CL
PE
PI/PS
PC

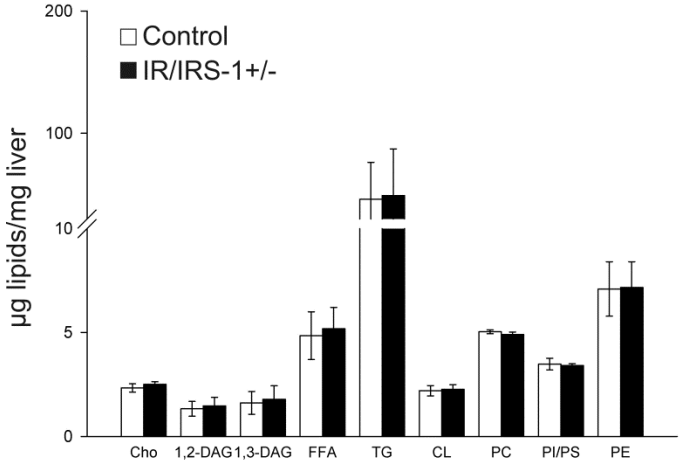
Control
IR/IRS-1+/-
µg lipids/mg liver
200
100
10
5
0
Cho
1,2-DAG
1,3-DAG
FFA
TG
CL
PC
PI/PS
PE

Suppl. Fig. 3

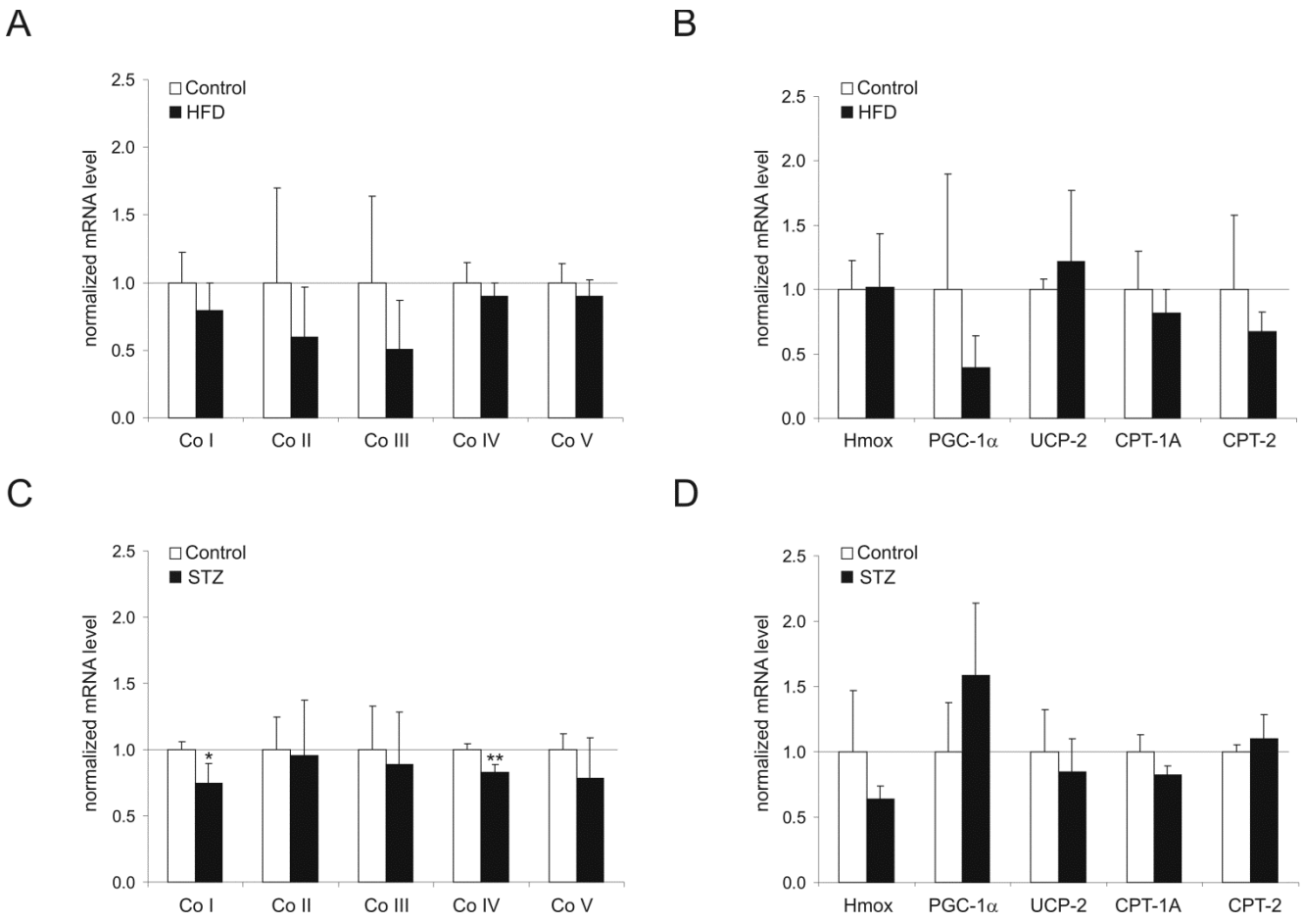
A
B
C
D
Control
HFD
STZ
normalized mRNA level
2.5
2.0
1.5
1.0
0.5
0.0
Co I
Co II
Co III
Co IV
Co V
Hmox
PGC-1α
UCP-2
CPT-1A
CPT-2
*
**

Suppl. Fig. 4

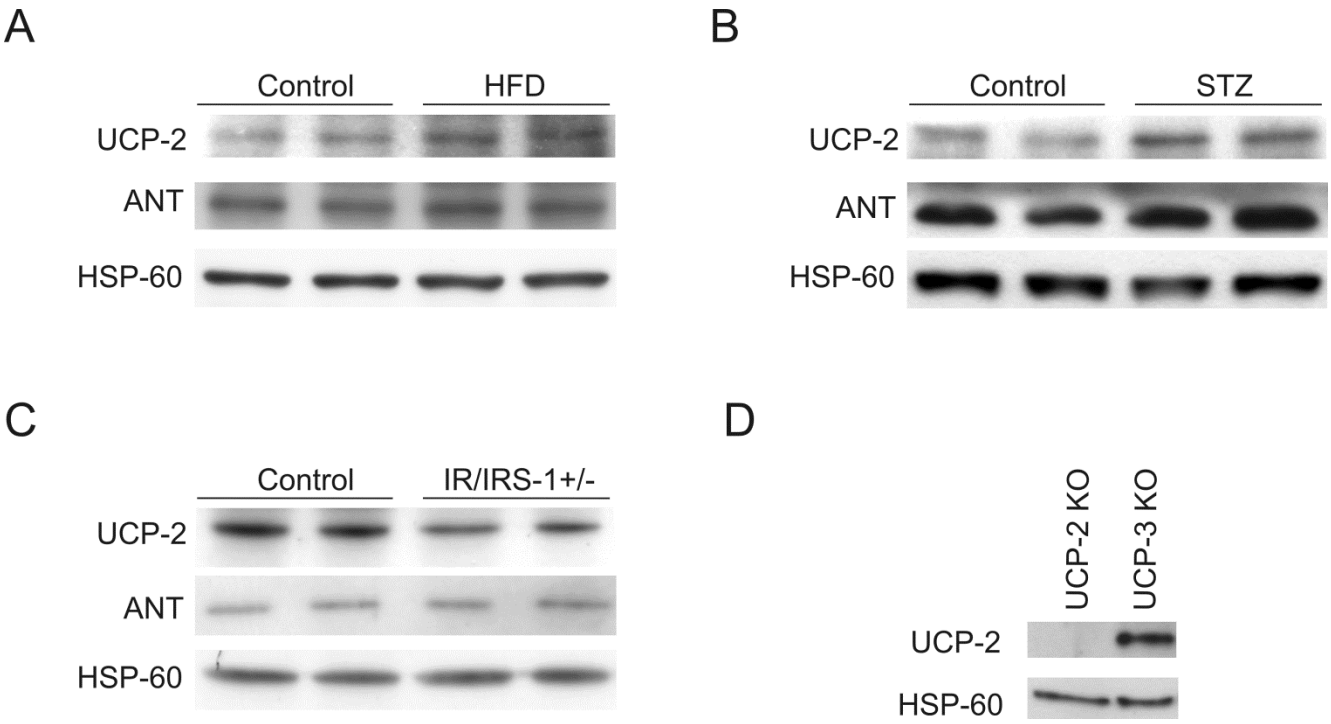
A
Control
HFD
UCP-2
ANT
HSP-60
B
Control
STZ
UCP-2
ANT
HSP-60
C
Control
IR/IRS-1+/-
UCP-2
ANT
HSP-60
D
UCP-2 KO
UCP-3 KO
UCP-2
HSP-60

Suppl. Fig. 5

Supplementary Table 1. State IV respiration of isolated liver mitochondria

State IV respiration was determined using pyruvate as a substrate (before the addition of ADP). Data are expressed as mean±SD, n=5-8, all differences were not significant. The given units are expressed in nmol O_2/ min x mg protein.

		State IV respiration
HFD	Control	7.61 ± 0.69
	Treated	7.81 ± 1.37
IR/IRS-1+/-	Control	7.20 ± 1.45
	IR/IRS-1+/-	6.20 ± 1.44
STZ	Control	6.80 ± 0.71
	Treated	7.90 ± 1.71

Supplementary Table 2. Normalized protein levels shown in Supplementary Fig. 5

Protein levels of UCP-2 and ANT were evaluated by densitometry and normalized to HSP-60 loading control. Data are expressed as mean±SD, n=4, **p<0.01

		UCP-2	ANT
HFD	Control	1.00 ± 0.17	1.00 ± 0.17
	Treated	1.17 ± 0.27	0.96 ± 0.05
IR/IRS-1+/-	Control	1.00 ± 0.04	1.00 ± 0.39
	IR/IRS-1+/-	0.74 ± 0.10 **	1.63 ± 0.50
STZ	Control	1.00 ± 0.36	1.00 ± 0.08
	Treated	1.38 ± 0.32	1.61 ± 0.24 **

Supplementary Table 3. Regulated transcripts in STZ treated mice

Global gene expression of liver from STZ treated and control mice was studied by microarray analysis. Significantly regulated genes were determined (FDR<10%) and selected genes are shown below. n=6-7

Gene symbol	Gene title	Entrez ID	Probe set	Linear ratio (STZ vs Ctrl)	Gene symbol
Slc16a5	solute carrier family 16 (monocarboxylic acid transporters), member 5	217316	10382532	**3.29**	**Slc16a5**
Ppargc1a	peroxisome proliferative activated receptor, gamma, coactivator 1 alpha	19017	10529979	**1.95**	**Ppargc1a**
Slc16a10	solute carrier family 16 (monocarboxylic acid transporters), member 10	72472	10368720	**1.69**	**Slc16a10**
Fabp7	fatty acid binding protein 7, brain	12140	10363224	**1.69**	**Fabp7**
Idh2	isocitrate dehydrogenase 2 (NADP+), mitochondrial	269951	10564857	**1.57**	**Idh2**
Cd36	CD36 antigen	12491	10528207	**1.55**	**Cd36**
Fabp4	fatty acid binding protein 4, adipocyte	11770	10497265	**1.52**	**Fabp4**
Pck1	phosphoenolpyruvate carboxykinase 1, cytosolic	18534	10479047	**1.50**	**Pck1**
Got1	glutamate oxaloacetate transaminase 1, soluble	14718	10467842	**1.50**	**Got1**
Slc25a12	solute carrier family 25 (mitochondrial carrier, Aralar), member 12	78830	10483604	**1.36**	**Slc25a12**
Me2	malic enzyme 2, NAD(+)-dependent, mitochondrial	107029	10459730	**1.32**	**Me2**
Gpt	glutamic pyruvic transaminase, soluble	76282	10424979	**1.30**	**Gpt**
Ogdh	oxoglutarate dehydrogenase (lipoamide)	18293	10374119	**1.26**	**Ogdh**
Mdh2	malate dehydrogenase 2, NAD (mitochondrial)	17448	10526381	**1.22**	**Mdh2**
Slc27a1	solute carrier family 27 (fatty acid transporter), member 1	26457	10572647	**1.20**	**Slc27a1**
Aco2	aconitase 2, mitochondrial	11429	10425611	**1.19**	**Aco2**
Pparg	peroxisome proliferator activated receptor gamma	19016	10540897	**0.57**	**Pparg**
Me1	malic enzyme 1, NADP(+)-dependent, cytosolic	17436	10595480	**0.30**	**Me1**
Gck	glucokinase	103988	10384051	**0.18**	**Gck**

Supplementary Information

Euglycemic-hyperinsulinemic clamps

An additional cohort of C57BL6/N (Taconic, Denmark) males was treated with a dose of 60 mg/kg STZ for three consecutive days and random-fed blood glucose concentrations monitored weekly thereafter. Five weeks, after STZ treatment permanent catheters were inserted into the left jugular vein and right carotid artery under surgical anesthesia (i.p. ketamine/xylazine = 80/10 mg/kg body weight). For the following 6-7 postsurgical days mice were closely monitored. Healthy, recovered, weight-matched (6-hour fasting body mass, g: STZ 23.6 ± 1.9 *versus* CON 25.4± 1.6, n.s.), and 6-hour fasting mice were subjected to euglycemic-hyperinsulinemic clamp experiments. Conscious, freely moving mice were placed in round containers (diameter ~20 cm) including home cage bedding after catheter ends were recovered from subcutaneous areas and connected to extension tubings used for blood sampling (arterial line) or infusions (venous line). For determination of 6-hour fasting (basal) whole-body glucose turnover rates (EndoRa) a primed-continuous [3-^{3}H]glucose infusion (0.05 µCi/min) was administered for 120 min and a blood sample for measurement of basal plasma glucose, insulin, and [3-^{3}H]glucose concentrations withdrawn in the final 10 minutes. To initate the euglycemic hyperinsulinemic clamp a continuous insulin infusion (2.5 mU/kg min^{-1}; Humulin R, Lilly, Indianapolis, USA) was started and continued for 120 minutes. To adjust “steady state” target glycemia blood glucose was measured every 10 min with a glucometer (Contour, Bayer, Leverkusen, Germany) and the rate of a 20% glucose solution varied accordingly. To account for increased glucose turnover the infusion rate of [3-^{3}H]glucose was raised to 0.1 µCi/min during insulin stimulation. Between min 90 and 120, four blood samples were

collected for calculation of insulin-mediated suppression of endogenous glucose appearance rates (endoRa), a marker of hepatic glucose production. All infusions were performed with microdialysis pumps (CMA 402, Axel Semrau GmbH, Sprockhävel, Germany) and radioisotopes were purchased from Perkin Elmer Life Sciences (Boston, MA, USA). Plasma glucose concentrations were determined *via* a glucose assay (LassAssay Glucose, Wako Chemicals GmbH, Neuss, Germany). Basal endoRa was calculated as the ratio of [3-^{3}H]glucose infusion rate and plasma [3-^{3}H]glucose specific activity. The endoRa during "steady state" insulin-stimulated conditions was determined by subtracting the Glucose Infusion Rate (GIR) from Rd. Plasma [^{3}-3H]glucose and $^{3}H_2O$ radioactivity were determined in deproteinized plasma samples (Somogyi filtrates) before and after $^{3}H_2O$ was completely evaporated. ^{3}H radioactivity was assessed in scintillation cocktail (Ultima Gold Scintillation Cocktail, PerkinElmer LAS, Rodgau-Juegesheim, Germany) using a Liquid Scintillation Counter (PerkinElmer Tri-Carb 2910TR).

Real time PCR

2 µg of total RNA were reversely transcribed (RT-PCR Master Mix, Eurogentec, Köln, Germany). Real-time PCR was performed using TaqMan Universal PCR Master Mix on an ABI Prism 7700 sequence detector (Applied Biosystems, Darmstadt, Germany). Specific primers and probes were purchased from Applied Biosystems. Calculations were done by a comparative method ($2^{-\Delta\Delta Ct}$). Results for mRNAs of interest were normalized to levels of the GUSB (glucuronidase, beta) mRNA as a "housekeeping gene", which remained unchanged according to absolute Ct values. The following TaqMan primers were used: Ndufa9-complex I: Mm00481216_m1, Sdha-complex II: Mm01352366_m1, Uqcrc2-complex III: Mm00445861_m1, Cox4i1-

complex IV: Mm00438289_g1, Atp5b-complex V: Mm00443967_g1, Hmox1: Mm00516005_m1, Ppargc1a: Mm00447183_m1, Ucp2: Mm00627599_m1, CPT1A: Mm00550438_m1, CPT2: Mm00487202_m1, Gusb: Mm00446953_m1.